Title	Impact-induced phyllosilicate formation from olivine and water
Auther(s)	Furukawa, Yoshihiro; Kakegawa, Takeshi; Sekine, Toshimori; Nakazawa, Hiromoto
Citation	Geochimica et Cosmochimica Acta , 75 (21) : 6461 - 6472
Issue Date	2011
DOI	10.1016/j.gca.2011.08.029
Self DOI	
URL	http://ir.lib.hiroshima-u.ac.jp/00034743
Right	(c) 2013 Elsevier Ltd.
Relation	

Available online at www.sciencedirect.com

SciVerse ScienceDirect

Geochimica et Cosmochimica Acta 75 (2011) 6461–6472

Geochimica et Cosmochimica Acta

www.elsevier.com/locate/gca

Impact-induced phyllosilicate formation from olivine and water

Yoshihiro Furukawa [a,*], Toshimori Sekine [b,c], Takeshi Kakegawa [a], Hiromoto Nakazawa [b]

[a] Department of Earth and Planetary Materials Science, Graduate School of Science, Tohoku University, Sendai 980-8578, Japan
[b] National Institute for Materials Science, Tsukuba 305-0044, Japan
[c] Department of Earth and Planetary Systems Science, Graduate School of Science, Hiroshima University, Higashi-Hiroshima 739-8526, Japan

Received 14 July 2010; accepted in revised form 19 August 2011; available online 26 August 2011

Abstract

Shock-recovery experiments on mixtures of olivine and water with gas (air) were performed in a previous study to demonstrate water–mineral interactions during impact events (Furukawa et al., 2007). The products of these former experiments were investigated in the present study using transmission electron microscopy, scanning electron microscopy, and X-ray powder diffraction with the aim of finding evidence of aqueous alteration. Serpentine formed on the surface of shocked olivine with well-developed mosaicism. The yield of serpentine depended on the water/olivine ratio in the starting material, indicating progressive serpentinization under water-rich conditions. Comminution and mosaicism were developed in shocked olivine grains. The temperature and pressure changes of the samples during the experiments were estimated by constructing Hugoniots for mixtures of olivine and water, combined with the results of an additional fracturing experiment on a shocked container. Pressures and temperatures reached 4.6–7.2 GPa and at least 230–390 °C, respectively, for 0.7 μs during in-shock compression. Post-shock temperatures reached a maximum of ~1300 °C, when the shock wave reached the gas in the sample cavity. The serpentine formed after the post-shock temperature maximum, most likely when temperatures dropped to between 200 and 400 °C. This is the first experiment to demonstrate the formation of phyllosilicates using heat supplied by an impact. The present results and estimations suggest that phyllosilicates could form as a result of impacts into oceans as well as by impacts on terrestrial and Martian crustal rocks, and on some asteroidal surfaces, where liquid or solid H_2O is available. A significant amount of phyllosilicates would have formed during the late heavy bombardment of meteorites on the Hadean Earth, and such phyllosilicates might have affected the prebiotic carbon cycle.

1. INTRODUCTION

The Earth has experienced numerous impact events by extraterrestrial bodies. Several impact structures have been recognized as having formed from impacts into oceans (e.g., Dypvik and Jansa, 2003). Depending on impact pressures, meteoritic projectiles may disrupt upon impact, even on water (Milner et al., 2008). Previous studies have indicated that projectile materials, water, and ambient atmosphere interact chemically in the post-impact plume formed by projectile impacts on water at an impact velocity of 5.9 km/s (Sugita and Schultz, 2003a,b). In such a water-bearing system, meteoritic minerals may undergo aqueous alteration. For example, serpentine is the typical aqueous alteration product of olivine and enstatite (Wegner and Ernst, 1983; Ohnishi and Tomeoka, 2007). Olivine and enstatite are the major constituent silicates in chondrites. Therefore, serpentine is one of the aqueous alteration products expected to result from oceanic impacts of meteoritic silicates.

Serpentine has been produced in a number of hydrothermal experiments (Yada and Iishi, 1974, 1977; Wegner and Ernst, 1983; Ohnishi and Tomeoka, 2007). According to Wegner and Ernst (1983), the reaction kinetics of serpentine formation depends on the nucleation and growth rates of

* Corresponding author. Tel./fax: +81 22 759 3453.
E-mail address: furukawa@m.tohoku.ac.jp (Y. Furukawa).

0016-7037/$ - see front matter © 2011 Elsevier Ltd. All rights reserved.
doi:10.1016/j.gca.2011.08.029

serpentine from forsterite (Mg_2SiO_4). Their results also suggest that the reaction rate is strongly dependent on the surface area of olivine grains and reaction temperatures between 200 and 400 °C (Wegner and Ernst, 1983).

The olivine in many meteorites is relatively rich in ferric iron, compared with the composition of terrestrial mantle olivine (e.g., Krot et al., 1997; Weisberg et al., 1997). The phase boundary between an iron-bearing olivine (($Mg_{0.9}$, $Fe_{0.1})_2SiO_4$) and serpentine is 15 °C lower than the phase boundary between forsterite and serpentine, under isobaric conditions (Moody, 1976). Thus, the depression of the phase boundary temperature may increase the reaction rate of iron-rich olivine to serpentine. In another hydrothermal experiment at 300 °C and 70 MPa, serpentine nuclei (identified using transmission electron microscopy, TEM) were produced within 30 min by hydrothermal reactions involving fine-grained olivine crystals (($Mg_{0.9}$, $Fe_{0.1})_2SiO_4$, 0.1–2 μm in diameter) (Yada and Iishi, 1977); these data indicate that serpentine can form quickly under suitable pressure–temperature conditions.

Several previous studies suggested that hypervelocity impacts promote the dehydration of phyllosilicates under water-poor conditions (Lange et al., 1985; Nakamura, 2005; Tomioka et al., 2007; Nakato et al., 2008). Gerasimov et al. (2002), in a laser ablation experiment simulating impact conditions, reported that phyllosilicates were not synthesized by interactions between augite and water vapor; these results did not, therefore, confirm that serpentine can be formed under shock conditions. In a previous study, we performed shock-recovery experiments combining olivine, water, and air in an encapsulated container, and demonstrated the formation of ultrafine particles of olivine and metal oxides (Furukawa et al., 2007). However, we did not examine whether phyllosilicates were synthesized. In the present study, the samples produced in this previous study were analyzed in detail using TEM, scanning electron microscopy (SEM), and X-ray powder diffraction (XRD), with the aim of investigating the possibility of phyllosilicate formation from water–olivine mixtures under shock conditions, and to discuss the conditions and implications of their formation in natural impact events.

2. MATERIALS AND METHODS

Our previous shock-recovery experiments were performed on mixtures of olivine and water using a single-stage propellant gun (Furukawa et al., 2007). The gun generates a shock wave by the hypervelocity impact of a steel plate (SUS304, 29 mm in diameter and 2 mm thick) onto a cylindrical steel sample container (SUS304, 30 mm in diameter and 30 mm long). The flyer-plate velocities ranged from 0.88 to 0.97 km/s. The sample container enclosed distilled water (Wako Pure Chemical Industries Ltd.) and powdered natural olivine (San Carlos, USA, consisting of ($Mg_{0.9}$, $Fe_{0.1})_2SiO_4$ with grain sizes of 10–100 μm) (Table 1). The containers were trimmed using a lathe to recover samples after the shock experiments. Because part of the inner wall of the sample container was slightly fragmented by the shock wave, some steel fragments were mixed with the sample and oxidized by water. To minimize water loss by this oxidation, for three shots (1011, 1012, and 1013) the inner surfaces of the sample container were covered with a 100-μm-thick gold shield. Two shots (1005 and 1010) were performed without the gold shield for comparison. Further details of the materials and methods employed in the shock-recovery experiments are described in a previous paper (Furukawa et al., 2007).

In the present study, we investigated the crystallinity of major minerals using XRD (X-Pert Powder; Philips Co.) with a Cu target. All diffraction profiles were obtained at a step size of 0.01°, with a divergence slit of 1° and a receiving slit of 0.3 mm. Particle morphology and sizes were observed using an SEM (JSM-6500F; JEOL) operated at an acceleration voltage of 3 kV. Fine-grained products were identified using a TEM (JEM 2010; JEOL) at an acceleration voltage of 200 kV with an EDS (Voyager II; NORAN Instruments). To prepare samples for TEM analysis, portions of the samples were dispersed in a bottle of ethanol using ultrasonic vibration. Small fragments were skimmed from the supernatant and mounted on a TEM grid with a thin carbon substrate. Very fine grains (less than ~1 μm) can be collected with this method; however, the sheet stacking normal to the *c*-axis of phyllosilicates could not be observed because the crystals were aligned parallel to the carbon substrate (i.e., vertical to the electron beam). The fine-grained fraction was observed in detail using bright-field TEM images (BFI), high-resolution TEM (HRTEM) images, selected area electron diffraction (SAED) data, and energy-dispersive X-ray spectrometry (EDS) data. Relative yields of phyllosilicates in the products were determined during the course of TEM observations based on the modal abundance of the phyllosilicate fragments.

When a shock wave propagates through the mixture and reaches the mixture–air interface, the olivine–water mixture expands adiabatically because of the low pressure of the shock wave reverberated at the boundary. We refer to the conditions immediately following shock compression as 'post-shock'. The sample containers burst when the impact velocity exceeded approximately 1.0 km/s, due to the post-shock internal pressure caused by the vaporization of water. Products analyzed in the present study were acquired from experiments conducted at velocities slightly below the burst-limit velocity.

The post-shock internal pressure at the burst can be estimated from the strength of the container material. In our previous studies, post-shock pressures were estimated using the tensile strength of steel (SUS304), supposing that the container burst by tensile failure (Nakazawa et al., 2005; Furukawa et al., 2007). However, estimates of the internal pressure based on the supposed tensile strength of steel may be unreliable, and the strength of such metal weakened by impact-related creep was unknown. Therefore, we conducted fracturing experiments on a shocked container and obtained a more realistic measurement of the strength of the steel weakened by impact creeping. The set-up of the fracturing experiment is illustrated in Fig. 1. After the shock experiment, a cut was made diametrically through the sample cavity to yield a disk containing the creep surface caused by impact (Fig. 1b). The expanded internal volume of the sample cavity was measured at this stage. In the

Table 1
Compositions of starting materials, impact conditions, and run products for the different runs (shots).

Shot no.	Sample			Impact conditions				Product
	Olivine (mg)	Water (μl)	Water content (wt.%)	Gold shield	Velocity (km/s)	Pressure (GPa)[a]	Temperature (°C)[b]	Serpentine[c]
1011	150	0	0.0	Yes	0.91	–	–	ND
1013	150	65	30.2	Yes	0.88	7.2	390	++
1012	150	130	46.4	Yes	0.90	6.4	340	+++
1005	151	130	46.3	No	0.97	7.1	380	+
1010	50	130	72.2	No	0.91	4.6	230	+++

[a] Water pressure during shock compression.
[b] Water temperature during shock compression.
[c] Relative yields of serpentine: ND, not detected; +, trace amounts (rarely found); ++, minor amounts (less than half of the large amount); +++, large amounts (frequently found; the number of serpentine particles on the TEM micro-grid exceeded that of olivine).

fracturing experiment, using a piston, we applied increasing amounts of pressure to the inner wall of the sample cavity of the disk until the disk fractured (Figs. 1b and c and 2), at which time the pressure was recorded.

3. RESULTS

3.1. Starting materials

TEM observations showed that phyllosilicates were not present in the starting material. In the XRD data, no peaks besides the sharp peaks for olivine could be detected (see Section 3.2 for a comparison with shocked samples). In the SEM images, all olivine grains showed sharp edges and smooth crystal surfaces. TEM observations of fine particles revealed that a minority of olivine crystals showed asterism spots in their SAED patterns, indicating the existence of a number of misoriented domains (i.e., mosaicism, Fig. 3). Such olivine grain mosaics can be formed through mechanical damage during preparation of the starting material (Brearley et al., 1992). However, such mosaicism was a minor phenomenon because most olivine grains in the starting material showed single-crystal features, as illustrated by their SAED patterns (Fig. 4).

3.2. The shocked water-free sample

Olivine was the only mineral identified by peaks in the XRD spectra of shocked samples. However, the olivine peaks showed significant broadening after impact relative to before (Fig. 5). Line broadening in XRD spectra is influenced by the size and the internal strain of the crystallites (Williamson and Hall, 1953). Fig. 6a shows the integral breadths of the olivine peaks in the starting materials and in shot 1011, plotted against the Bragg angle (2θ), compared with similar data for standard polycrystalline silicon (integral breadth = 0.13°; solid line). These plots suggest that the olivine in the starting material did not possess significant internal strain, and that crystallite sizes were sufficiently large not to show significant line broadening. In a Williamson–Hall plot of the olivine peak for shot 1011 (Fig. 6b), where B represents the difference between the integral breadths of the standard and the samples (Williamson and Hall, 1953), $B\cos\theta$ increases with $\sin\theta$; the intercept of the $\sin\theta$–$B\cos\theta$ regression is $B\cos\theta = 0.001$–0.003. These data indicate that the crystallite sizes of the shocked olivine was 50–160 nm, and that the olivine was strained. The reduction in crystallite size reflects the formation of inter- and intragranular fractures or mosaicism. Because the olivine in the starting material was powdered, the intragranular fracturing represents comminution. Broadening of olivine peaks due to shock pressure has been reported in a previous study (Hanss et al., 1978).

The experimental peak shock pressures (4.6–7.2 GPa) correspond to shock stage S2 of Stöffler et al. (1991). It has been reported that irregular fracturing becomes dominant in olivine in shock stage S2, based on optical microscopic observations (Reimold and Stöffler, 1978; Stöffler et al., 1991). The XRD data of the shocked samples of the present study are consistent with the occurrence of such shock fracturing.

SEM observations indicate that all the shocked olivine grains had sharp edges and were associated with smooth crystal surfaces. Phyllosilicates were not observed by TEM. The TEM observations of olivine particles revealed significant differences in their crystallinity (Fig. 7). Most of the fine-grained shocked olivine showed marked asterism in their SAED patterns, indicative of mosaicism.

Previous shock experiments at 56 GPa on olivine (Jeanloz et al., 1977) and 45 GPa on diopside (Leroux et al., 1994) indicated that SAED asterism spots stemmed from shock-induced mosaicism. Mosaicism of olivine is generally predominant in samples shocked above 20 GPa (Reimold and Stöffler, 1978). However, Brearley et al. (1992) reported that mosaicism in olivine can result from mechanical crushing during sample preparation, although only to a small degree. Therefore, the mosaicism observed in the present samples might be caused by preferential fracturing into the fine particles, rather than by homogeneous plastic deformation in larger olivine crystals.

3.3. Water-bearing samples after impact

The XRD peaks of shocked olivine grains were broadened, similar to the peaks of olivine in the water-free sample (see Fig. 5). In TEM observations, electron diffraction spots of most of the fine olivine grains showed marked asterism, indicative of mosaicism. SEM observations indicate that

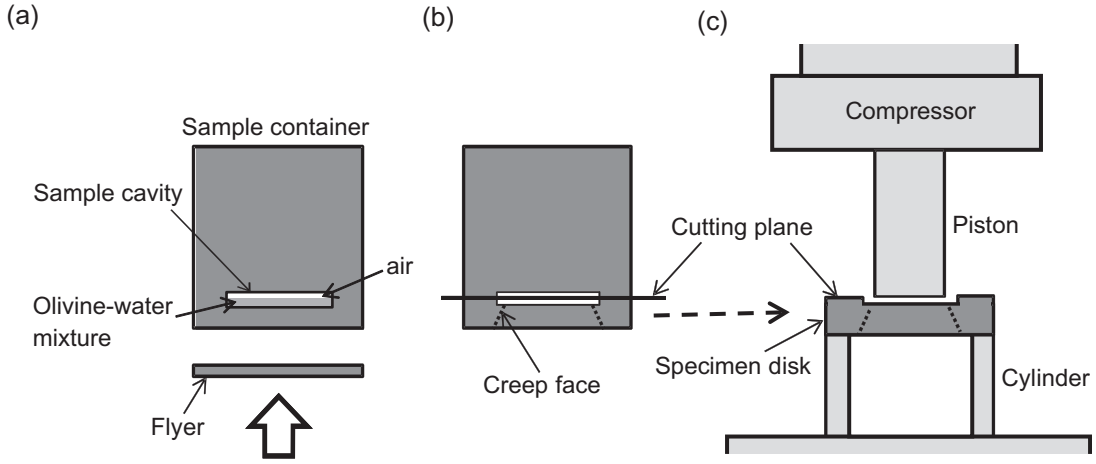

Fig. 1. Experimental set-up for the fracturing experiment with the shocked container. (a) Sample container before impact. (b) Sample container after impact. A cone-shaped creep face formed in the wall between the sample cavity and the impacted face. The container was cut on a plane traversing the sample cavity to produce a disk suitable for strength testing. (c) Set-up of the fracturing experiment: the specimen disk was placed on a cylinder and then pressed by a piston on the exposed inner side of the sample cavity until the disk fractured.

parts of the shocked olivine grains were covered with thin feather-like particles less than 10 nm long, which were not found in the starting material or the water-free shocked sample (Fig. 9). The HRTEM images (Fig. 10) show sheet-like particles that correspond to the thin feather-like material observed in SEM images (Fig. 9). The SAED patterns (Fig. 10b and d) are composed of hk0 spots of serpentine or talc. The diffractions from (001) are not apparent in these SAED patterns because the sheets were preferentially oriented vertical to the electron beam. That is because the sheet-like products were dried after the suspension had been mounted on the TEM micro-grid. Although the sheets are partly turned, the thicknesses of the sheets were insufficient for apparent diffraction. Therefore, we were not able to observe the lattice spacing of sheet stacking normal to the electron beam (i.e., the *c*-axis of the phyllosilicates).

The chemical composition of the sheet-like products was determined using EDS on typical grains (Fig. 10a and c) and assemblages (Fig. 8; Table 2). The composition was identical to that of serpentine and excluded the possibility of talc. All information from the SAED patterns and chemical compositions indicate that the sheet-like products were poorly crystallized serpentine. Such serpentine was found in all four water-bearing shocked samples, but was absent in the starting material and in the water-free shocked sample.

Relative yields of serpentine were determined by the modal abundance of the serpentine fragments, although the yields cannot be quantitatively expressed due to the heterogeneous distributions of the samples on the TEM micro-grids and due to the sample collection protocol. The relative yields of serpentine in gold-shielded and shield-free runs were roughly proportional to the water content in

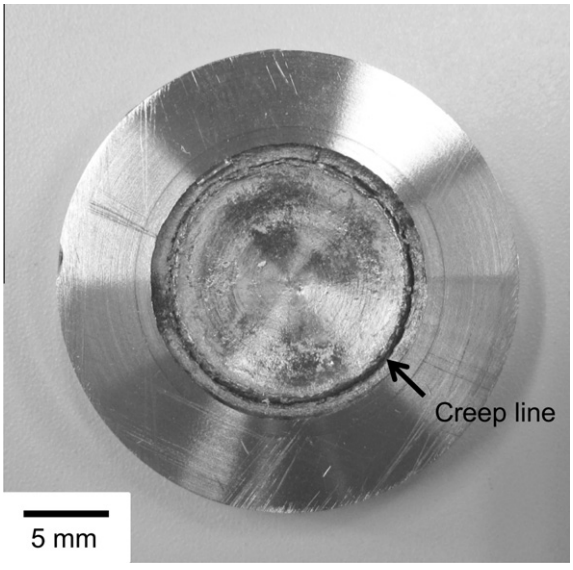

Fig. 2. Specimen disk before the fracture experiment. The disk has a circular creep line on the side of the sample cavity.

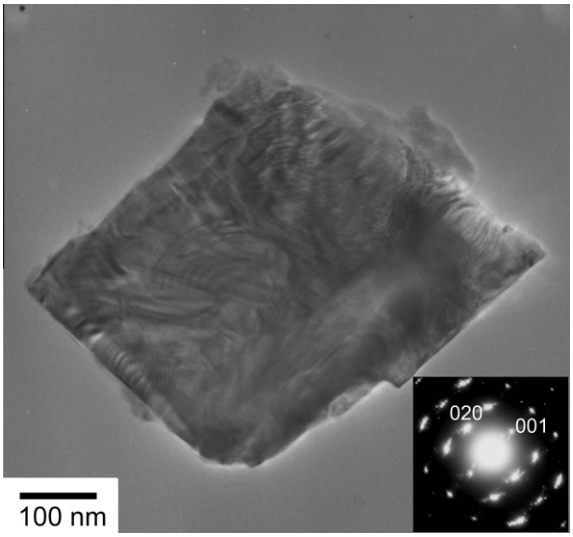

Fig. 3. High-resolution transmission electron microscopy image of an olivine grain in the starting material. The grain shows heterogeneous diffraction contrasts and moiré patterns. Each spot in the SAED pattern (inset) shows marked asterism.

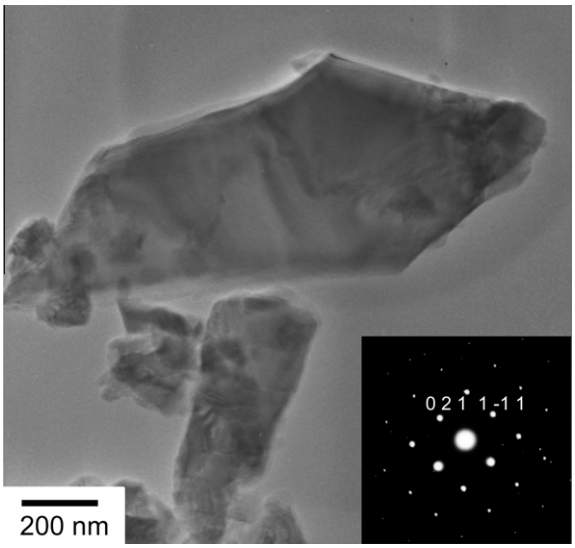

Fig. 4. High-resolution transmission electron microscopy image of a very weakly strained olivine grain in the starting material. The grain shows a slightly heterogeneous diffraction contrast. The SAED pattern (inset) shows a set of discrete diffraction spots from a single crystal.

the starting materials (Table 1). When the water/olivine ratio was doubled, the relative yields of serpentine approximately doubled in the gold-shielded samples (shots 1013 and 1012). Among the samples without gold shield, when the value of the water/olivine ratio was increased by a factor of three, the relative yields of serpentine increased by more than a factor of two (shots 1005 and 1010). The gold shield affected the relative yields because it prevented water from being consumed by the oxidation of the container material. This is reflected in the fact that the relative yields of serpentine were not the same in samples with the same water/olivine ratio (shots 1012 and 1005); the high yield sample (shot 1012), and the low yield sample (shot 1005).

3.4. Fracturing experiments on a shocked container

Through the impact experiments, the inside volume of the sample container decreased from 890 mm^3 to 280–340 mm^3. In the fracture experiments, when the clipped disk was subjected to a pressure exceeding 340 MPa, it was fractured into a ring and a smaller disk penetrated by the piston. The fractured faces were similar to those caused by impact bursting, showing slick lustrous surfaces. This pressure limit of fracturing constrains the internal maximum pressure of the sample container under post-shock conditions.

4. DISCUSSION

4.1. Estimation of pressure and temperature changes during the in- and post-shock conditions

Samples enclosed in a container and subjected to hypervelocity impacts experience a variety of in-shock and post-shock physical and chemical processes. Fig. 11 shows estimated pressures (P) and temperatures (T) that accompany

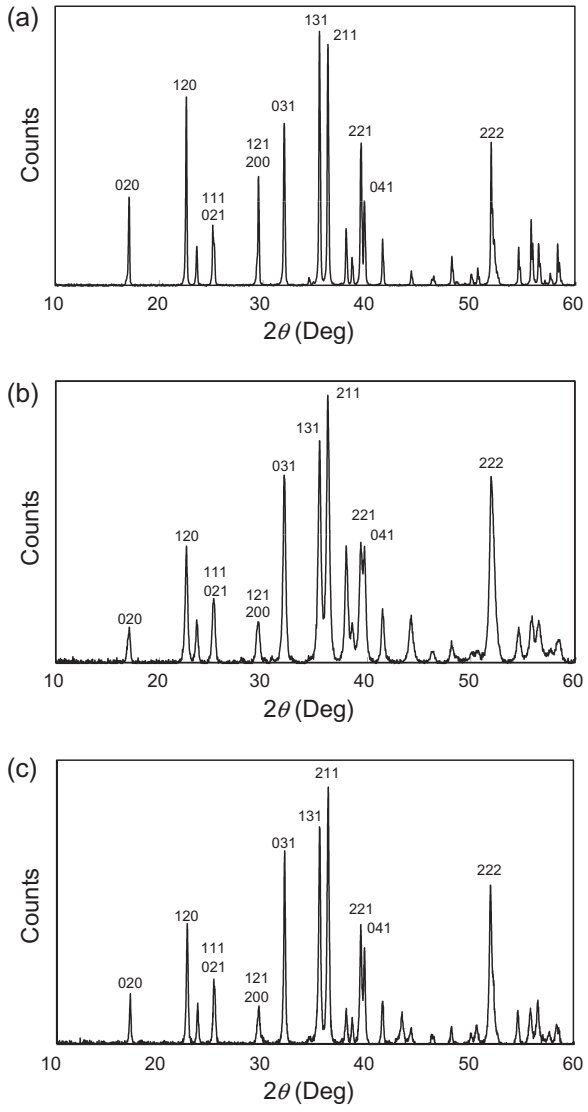

Fig. 5. (a) X-ray diffraction (XRD) pattern of olivine in the starting material. (b) XRD pattern of water-free shocked product from shot 1011. (c) XRD pattern of water-bearing shocked product from shot 1005.

shock events, represented schematically on a serpentine phase diagram (Ulmer and Trommsdorff, 1995; Irifune et al., 1998). Pressure and temperature show rapid increases from the initial pre-shock to the in-shock condition (<0.1 μs) due to the high velocity of the shock wave in water (Rice and Walsh, 1957). The in-shock pressure was estimated using the impedance match method with known Hugoniots for the projectile and target. The Hugoniots for San Carlos olivine and water are expressed as $U_s = 6.57 + 0.85U_p$ (km/s) and $U_s = 1.48 + 1.86U_p$ (km/s), respectively, where U_s is the shock-wave velocity and U_p is the particle velocity (Rice and Walsh, 1957; Brown and Furnish, 1987). To estimate the in-shock pressures, we calculated the U_s–U_p relations for the sample itself, assuming volume additivity of olivine and water (Fig. 12). Using the U_s–U_p relations, the peak pressure was calculated at 4.6–7.2 GPa.

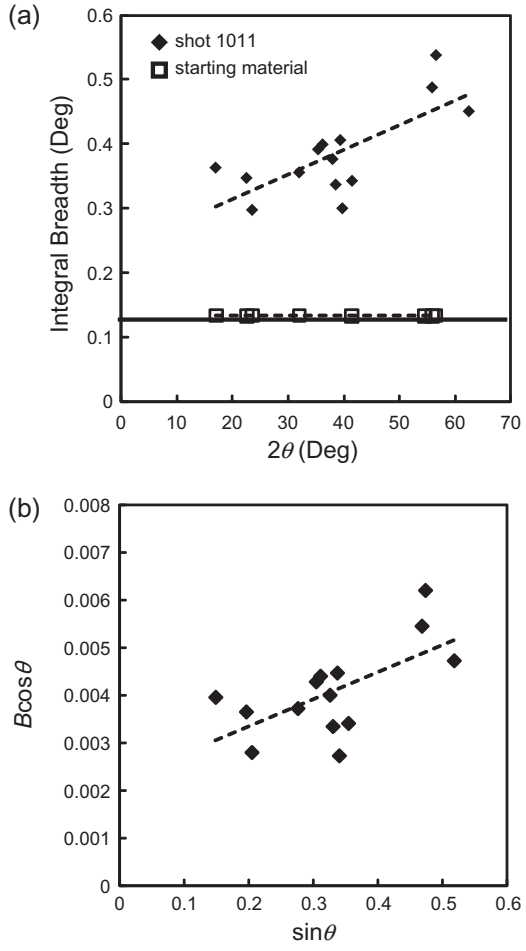

Fig. 6. Plots of olivine peaks in X-ray diffraction spectra. (a) Integral breadths of olivine peaks in starting material (squares) and in shocked product from shot 1011 (diamonds). Dashed lines are the regression lines for these data ($R^2 = 0.53$). The solid line is the integral breadth of standard polycrystalline silicon. (b) Williamson–Hall plot of olivine in shot 1011. The dashed line is the regression line through the data ($R^2 = 0.40$). θ = Bragg angle; B = difference of integral breadths between standard and samples calculated assuming a Lorentzian approximation.

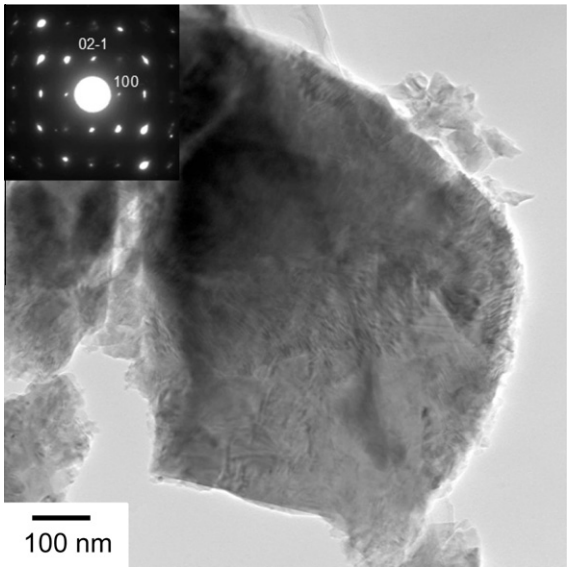

Fig. 7. High-resolution transmission electron microscope (HRTEM) image and selected area electron diffraction (SAED) pattern (inset) of olivine in the water-free sample (shot 1011). The olivine grain shows significant heterogeneous diffraction contrasts, and a moiré pattern. Each spot in the SAED pattern shows marked asterism.

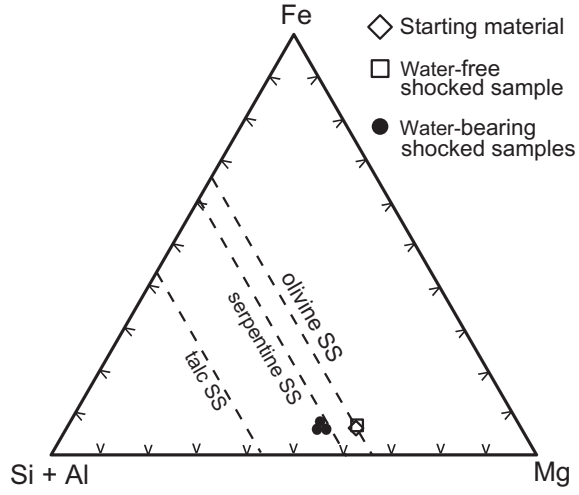

Fig. 8. Ternary Si + Al–Fe–Mg plot for serpentine-like products and a grain shown in Fig 10a. Dashed lines represent solid solutions of olivine, serpentine, and talc.

The temperature of water was calculated to 230–390 °C during shock compression (Table 1), based on the estimated sample pressures and known P–T relationships for water (Rice and Walsh, 1957). This estimation probably represents the minimum temperature during shock compression, because some of the chemical and mechanical interactions among the sample materials caused additional heating, as indicated by the estimates of post-shock temperatures. The in-shock duration for the present olivine–water mixtures was estimated at approximately 0.7 μs using the shock wave velocity in water (Rice and Walsh, 1957).

In the post-shock period, a shock wave reached the gases that filled the space between the sample mixture and the container wall (Fig. 1a). At that time, the container bursts when the impact velocity exceeds ~1 km/s. Based on the fracturing experiments, the inner pressure of the container at the time of bursting was an estimated 340 MPa. Based on the inner pressure and the volume of the sample container (280–340 mm^3), the temperature of water in the container was estimated at 1300–1600 °C, assuming ideal gas behavior. Because shock-recovery experiments were conducted at a velocity slightly below the burst limit, the post-shock maximum temperature should have been less than 1300 °C. This strong heating was probably caused by the high compressibility of gas, as well as chemical and mechanical interactions among high-speed impactor fragments, water vapor, and air (Sugita and Schultz, 2003a,b). In this case, the post-shock temperature probably increased very quickly (within

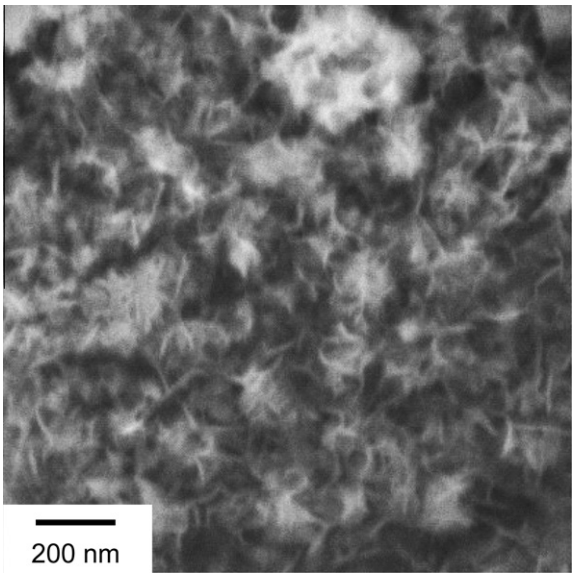

Fig. 9. Scanning electron microscope image of phyllosilicate-like material formed on olivine from shot 1010. This material was only found in the water-bearing samples.

~1 μs). After reaching the post-shock maximum *P–T* condition, the sample container cooled to a temperature of between 40 and 70 °C in about 10 min. Based on these cooling time and temperature constraints, the residence time of samples at 200–400 °C was estimated at ~2 min, assuming exponential cooling by thermal conduction. Wegner and Ernst (1983) reported that reaction rates of serpentinization are rapid in this thermal range. We consider that such thermal conditions associated with supercritical or subcritical states of water were important for serpentine formation in our experimental products.

4.2. Mechanism of shock-induced serpentinization

Impact heating changes water to supercritical and subcritical conditions. The lower viscosity of the super- and subcritical water results in high diffusivity into solid materials. Such water dissolves or alters materials at a much higher rate than water at comparatively lower temperatures (Becker et al., 1983; Adschiri et al., 1992; Sasaki et al., 2000).

X-ray diffraction data from this study indicate that the diameters of most olivine crystallites were decreased in the experiments from approximately 10–100 μm to 50–160 nm, due to fracturing or mosaicism induced by the shock wave (Fig. 7b). Previous studies reported that fracturing is dominant over mosaicism at shock pressures in the range from 5 to 20 GPa (Reimold and Stöffler, 1978; Stöffler et al., 1991). Thus, the surface area of the shocked olivine was much larger than that of the olivine in the starting material, thereby increasing the rate of serpentinization.

The increase in strain demonstrated by the Williamson–Hall plot (Fig. 7b) suggests that the abundance of dislocations and mosaicism in olivine crystals were increased by shock. Kohlstedt et al. (1976) reported a high diffusion rate of oxygen along dislocations in olivine.

Smectite was found along fractures in the Martian meteorite, Nakhla (Bridges and Grady, 2000). In hydrothermal experiments, saponite was formed along defects of olivine in a meteorite matrix (Keller et al., 1994). These findings indicated that the development of dislocations and mosaicism increases the rate of serpentinization and enhances the diffusion of water, Si, Fe, O, and Mg within olivine crystals, although the formation of serpentine along dislocations was not directly observed.

Yada and Iishi (1977) performed experiments involving the hydrothermal serpentinization of fine-grained olivine crystals (diameter, 0.1–2 μm; composition $(Mg_{0.9}, Fe_{0.1})_2SiO_4$) at 300 °C and 70 MPa for 30 min. They synthesized nuclei of serpentine, but the serpentine nuclei were only detectable by TEM and not by XRD. The crystallinity and shape of serpentine observed in the present study is similar to that observed in their products. The presence of shocked textures in olivine and the availability of super- to subcritical water may explain the differences in reaction rates between our experiments and the experiments by Yada and Iishi (1977).

Shock-induced aqueous alteration reactions may also apply to other silicates. Impact disruption and shock-induced microstructures in silicates other than olivine (e.g., quartz, plagioclase, and enstatite) has been reported in many previous studies (e.g., Stöffler et al., 1991; Langenhorst et al., 1995). Therefore, during impact events, interaction of water with olivine and other silicates would be expected.

4.3. Extrapolation to natural impacts

4.3.1. Pressure range applicable to natural oceanic impacts

A previous experimental study indicated that the temperature of an ice–quartz mixture changed from 100 to 360 K during post-shock conditions due to an impact that generated an in-shock pressure of 7.9 GPa (Kraus et al., 2010). This temperature change corresponds to the phase change from ice to liquid water. At 18.5 GPa, post-shock temperatures increased to 660 K, which is associated with the phase change to supercritical fluid (Kraus et al., 2010). Therefore, impact pressures greater than 20 GPa in natural impacts would be sufficient to generate serpentine-forming temperatures, even in the absence of heat sources generated by chemical and mechanical interactions, as in the present study. A simple calculation, based on the impedance match calculation, indicates that an impact pressure of 20 GPa is realized when an ordinary chondrite (represented by the Hugoniot of Jilin) impacts on water at a velocity of 4.0 km/s (Dai et al., 1997).

Regarding the present samples, the residence time of water heated to between 200 and 400 °C would be the limiting factor for the generation of serpentine, because serpentine was formed during the temperature-decreasing period following the post-shock temperature maximum (Fig. 11). The residence time of such heated water in the present experiments was estimated at only a few minutes, mainly because of the high diffusivity of heat in the metallic

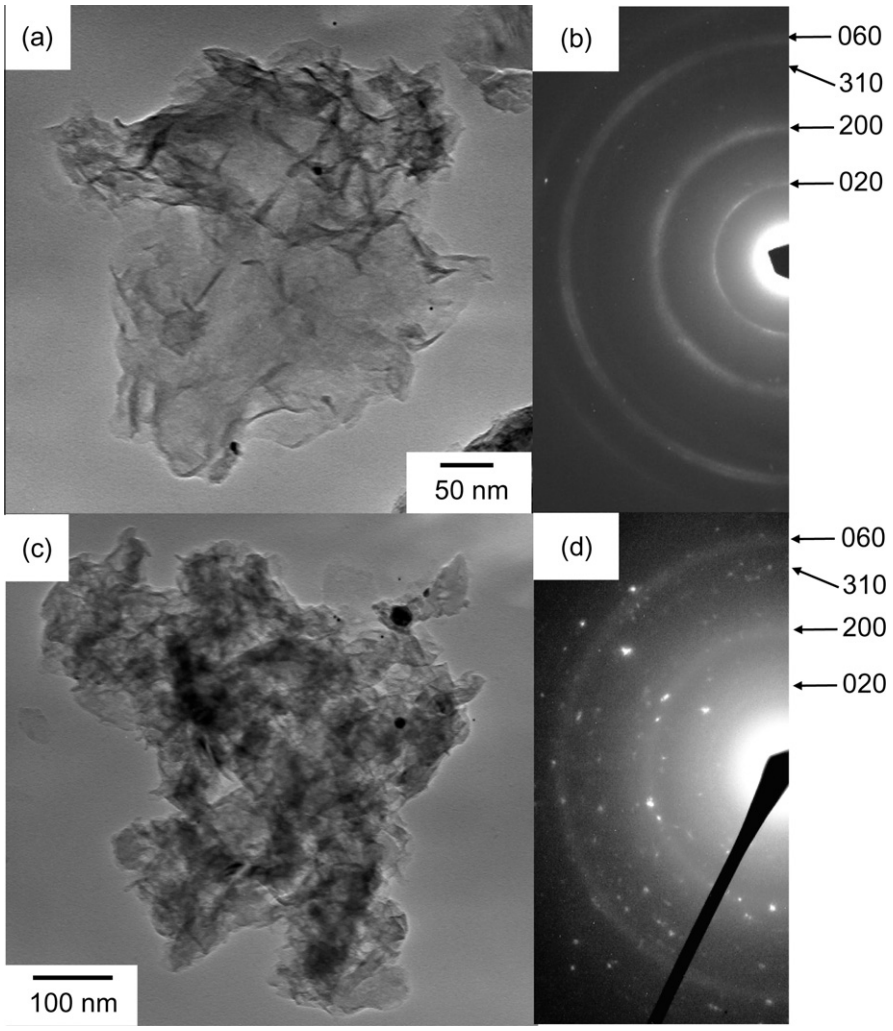

Fig. 10. High-resolution transmission electron microscope (HRTEM) images and selected area electron diffraction (SAED) patterns of typical serpentine-like product grains from shot 1012. (a) HRTEM image of a product grain showing sheet-like morphology. (b) SAED pattern of the grain in Fig. 10a. The pattern is composed of broad rings. (c) HRTEM image of an aggregation of sheet-like grains from shot 1012. (d) SAED pattern of the aggregation in Fig. 10c.

Table 2
Energy-dispersive X-ray spectrometry (EDS) data acquired to determine the compositions (atomic ratios) of serpentine and olivine found in the water-free sample and water-bearing samples.

	k-factor[a]	Analytical point				
		#1 (shot 1013)	#2 (shot 1013)	#3 (shot 1012)	#4 (shot 1011)	#5 (shot 1011)
Mg	1.00	53	50	50	59	58
Si	0.64	41	43	42	34	33
Fe	0.61	5	6	8	7	9
Total[b]		100	100	100	100	100

[a] Standardless EDS analyses were performed using these Cliff–Lorimer sensitivity factors (i.e., *k*-factor).

[b] Only the data for Mg, Si, and Fe are shown. Although chromium was detected at below 1 at %, it was not quantified. Aluminum was not detected in any sample. A ternary plot of these data is shown in Fig. 8.

container. Heat diffusion rates in the terrestrial atmosphere, ocean, and crustal rocks are expected to be much less than those of the metallic container. Therefore, the residence time of water between 200 and 400 °C will likely be longer than 2 min during natural impacts. Longer residence times are expected in the case of high impact velocities and large projectile sizes.

Many previous studies on shock effects of minerals agree with the general correlation between shock pressure and fracturing (e.g., Müller and Hornemann, 1969; Madon and Poirier, 1983; Langenhorst et al., 1995; Joreau et al., 1997). Such impact fracturing enhances the rate of serpentinization because of the larger surface area available for reactions. For example, impact experiments involving metal projectiles on water have indicated that 70% of the mass of the projectile is comminuted at impact velocities greater than 3 km/s (Milner et al., 2008). In the case of impact between an ordinary chondrite, such as Jilin, and water, an impact of 3 km/s generates a shock pressure of

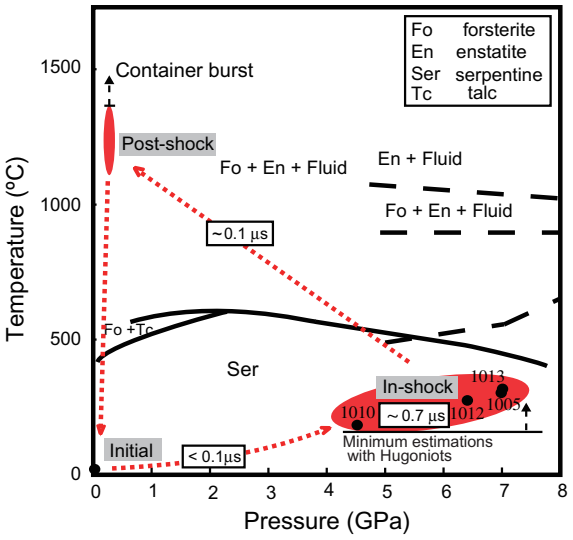

Fig. 11. Pressure and temperature transitions shown on the phase diagram of serpentine. Dotted arrows show *P–T* transitions of samples. Solid lines (Ulmer and Trommsdorff, 1995) and dashed lines (Irifune et al., 1998) show the phase boundaries. The numbers shown in the in-shock represents shot numbers. The temperatures during shock compression are minimum values.

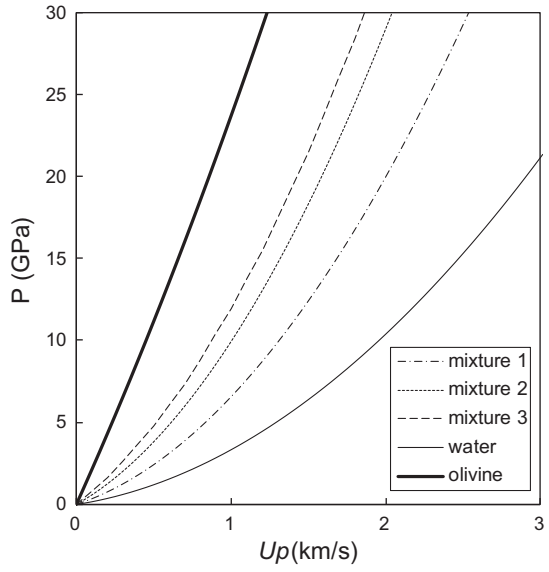

Fig. 12. Hugoniots for olivine, water, and mixtures. Mixture 1 (shot 1013) contained 150 mg olivine and 65 mg water. Mixture 2 (shots 1005 and 1012) contained 150 mg olivine and 130 mg water. Mixture 3 (shot 1010) contained 50 mg olivine and 130 mg water.

12.8 GPa (Dai et al., 1997). This pressure would be sufficient for microstructural alteration and the formation of shock fracturing in many silicates.

The velocities of extraterrestrial objects are reduced by atmospheric friction in natural impacts, depending on the sizes of projectiles. In the case of small meteorites, the velocity reduction is substantial. Therefore, micrometeorites cannot generate hypervelocity impacts, nor can the impact conditions result in the formation of phyllosilicates. On the other hand, micrometeorites may be easily altered in oceanic impacts because of their high ratio of surface area to volume.

4.3.2. Impact-induced interactions between crustal materials and H_2O

When the crust at an impact site contains water, hydrothermal activity may be generated by the impact; such processes in terrestrial impact structures have been reported in previous studies (e.g., Ames et al., 1998; Osinski et al., 2005; Abramov and Kring, 2007). Silicates in crustal materials are commonly fractured when affected by shock waves (e.g., Ferrière et al., 2008). Impact heating and fracturing can create conditions suitable for aqueous alteration of crust. Indeed, phyllosilicates have been found in terrestrial impact strata that record post-impact hydrothermal activity (Naumov, 2005). Impact events on water-rich crust may generate conditions similar to the post-shock conditions of the present samples, in which shock heating and fracturing were applied to a silicate–water mixture. Therefore, the present study may be applicable to the genesis of phyllosilicates related to post-impact hydrothermal activity.

Post-impact hydrothermal activity on Mars has been proposed previously (e.g., Schwenzer and Kring, 2009; Barnhart et al., 2010; Marzo et al., 2010; Ivanov and Pierazzo, 2011). Some nakhlites contain iddingsite (an assemblage of phyllosilicates, carbonates, sulfates, and iron hydroxides) along fractures in olivine (Treiman et al., 1993; Bridges and Grady, 2000; Noguchi et al., 2009; Changela and Bridges, 2010). Shock pressures of the nakhlites Lafayette and Y-000593 have been estimated at 5–10 GPa based on shock metamorphism of constituent olivine and pyroxene (Fritz et al., 2005). In addition, refractive indices of plagioclase in Nakhla and Governador Valadares suggest impact pressures of 14–20 GPa (Fritz et al., 2005). In impacts on ice, a shock pressure over 5 GPa transforms 100 K ice into liquid water under post-impact conditions (Stewart and Ahrens, 2005). Treiman et al. (1993) suggested that iddingsite on Mars most likely formed at 323–373 K. The results of these previous studies imply that some of the phyllosilicates on Mars formed as a result of post-impact hydrothermal activity. The present results support this hypothesis, by providing experimental evidence for serpentine formation from a mixture of olivine and water during an impact event.

The aqueous alteration of olivine in combination with other silicates, such as augite, may yield clay minerals such as saponite, which is commonly reported in carbonaceous chondrites (e.g., Tomeoka and Buseck, 1988; Nakamura et al., 2003). Phyllosilicates are found in many carbonaceous chondrites of types 1–3 (Tomeoka and Buseck, 1988, 1990; Keller and Buseck, 1990; Brearley, 1997). One proposed model, especially for the origin of fine-grained phyllosilicates in chondrule rims, is related to the interaction of chondrules with water vapor in a nebula, induced by shock heating (Ciesla et al., 2003). In addition, many previous studies have suggested that the decay of ^{26}Al is a major heat source that stabilizes liquid water in asteroids and that contributes to the formation of phyllosilicates (Macpherson et al., 1995; Brearley, 2006). On the other

hand, impact energies have been proposed as a temporal heat source that stabilizes water in asteroids (Grimm and McSween, 1989). A previous experimental study indicates that hypervelocity impacts on ice at shock pressures above 5 GPa transform 100 K ice into liquid water under post-shock conditions (Stewart and Ahrens, 2005). A number of shocked minerals in meteorites indicate that large amounts of asteroids experienced impact pressures of >5 GPa (e.g., Scott et al., 1992). Therefore, the present results imply that hypervelocity impacts could be a mechanism of phyllosilicate formation on ice-rich asteroids.

4.3.3. Implication for the late heavy bombardment on the hadean earth

The formation of phyllosilicates as a result of impacts might have affected prebiotic carbon cycles. Continental and seafloor weathering on the Earth are two major processes involving the aqueous alteration of minerals. Geochemical evidence suggests that large parts of continental crust most likely formed after 3.8 Ga (Martin, 1994; Taylor and McLennan, 1995). This implies an extremely small flux of phyllosilicates into Hadean marine environments from continental weathering. Conversely, seafloor weathering or hydrothermal alteration of oceanic crust would have been an alternative source of phyllosilicates on the Hadean Earth. Some investigators have estimated the conversion rate of modern abyssal peridotite into serpentinite using the Mg budget (Snow and Dick, 1995); the estimated conversion rate translates to a phyllosilicate yield of 1.41×10^{21} g for the time interval 4.0–3.8 Ga, based on the following three assumptions: (1) Mg-rich ultramafic rocks, such as komatiite, were major sea floor components; (2) serpentinization was caused by hydrothermal alteration or seafloor weathering; and (3) the rate of oceanic lithosphere movement and the thickness of the altered layer at that time were the same as today.

It has been suggested that a period of intense impact activity, the so-called Late Heavy Bombardment, occurred during the late Hadean, between 4.0 and 3.8 Ga (e.g., Culler et al., 2000; Valley et al., 2002). The flux of extraterrestrial materials on Earth between 4.0 and 3.8 Ga has been estimated at 1×10^{23} to 2×10^{23} g (Schoenberg et al., 2002). Given that the presence of an ocean well before 3.8 Ga has been suggested (Wilde et al., 2001; Cavosie et al., 2005), oceanic impacts were probably common during this geological period. A high flux of meteoritic projectiles implies that substantial amounts of impact-formed phyllosilicates were supplied into early oceans and affected silicate cycles on the surface of the Hadean Earth.

The prebiotic ocean is often considered the site of the chemical evolution that led to the origin of life (Miller, 1953; Cronin and Moore, 1971; Mukhin et al., 1989; Cronin and Pizzarello, 1997; Huber and Wächtershäuser, 2006; Nakazawa, 2006; Proskurowski et al., 2008; Furukawa et al., 2009). However, the extremely low concentration of organic molecules, such as amino acids, in the oceans presents an important problem for prebiotic polymerization (Cleaves et al., 2009). Bernal (1949) proposed that phyllosilicates were an effective substrate for the concentration of organic molecules. Later, many researchers demonstrated the role of phyllosilicates as substrates for organic concentration and as catalysts for peptide formation (Hedges and Hare, 1987; Ferris et al., 1996). Because phyllosilicates formed on the deep seafloor contribute little to the mass of organic substrate in the ocean, and because the flux of phyllosilicates from the continents was much less on the early Earth, impact-formed phyllosilicates might have played an important role as a substrate for organic concentration and as a catalyst for their polymerization. It is possible that phyllosilicates affected prebiotic carbon cycles by enhancing the flux of organic carbon from seawater to seafloor sediments.

5. CONCLUSIONS

Detailed TEM observations of the products of shock-recovery experiments on olivine and olivine–water mixtures has demonstrated the formation of impact-induced serpentine. The yield of serpentine depends on the water/olivine ratio in the starting materials; higher yields of serpentine are found in samples with higher water/olivine ratios. Numerical calculations based on the Hugoniots of the sample materials, and measurements of the container strength after impact, indicate that water transforms to super- and subcritical phases; the temperature of the water decreased with time during post-shock conditions. Significant comminution and an increase in mosaicism were observed in fine olivine particles after shock experiments. The shock-induced comminution and mosaicism might have contributed to the rapid alteration of olivine to serpentine, facilitated by reactions with water heated to between 200 and 400 °C. The duration of serpentine formation was most likely restricted to a few minutes under these temperature conditions. The present results suggest that significant amounts of phyllosilicates might have formed in the oceans of the early Earth by impact events, possibly affecting prebiotic carbon cycles. The present results also suggest the possibility of an impact origin of phyllosilicates in H_2O-bearing rocks on Earth, Mars, and on asteroids.

ACKNOWLEDGEMENTS

We thank T. Kobayashi, T. Nagase, T. Otake, T. Nakamura, and M. Arakawa for assisting with experiments and for many valuable discussions. We gratefully acknowledge W.U. Reimold, A. Brearley, J. Bridges, A. Greshake, and anonymous reviewers for their editing and constructive reviews. This work was supported by grants to Y.F. and T.K. by the Japan Society for the Promotion of Science (No. 19·5159, 21·244080) and by the Tohoku University Global Center of Excellence Program, 'Global Education and Research Center for Earth and Planetary Dynamics'.

REFERENCES

Abramov O. and Kring D. A. (2007) Numerical modeling of impact-induced hydrothermal activity at the Chicxulub crater. *Meteorit. Planet. Sci.* **42**, 93–112.

Adschiri T., Kanazawa K. and Arai K. (1992) Rapid and continuous hydrothermal crystallization of metal-oxide particles in supercritical water. *J. Am. Ceram. Soc.* **75**, 1019–1022.

Ames D. E., Watkinson D. H. and Parrish R. R. (1998) Dating of a regional hydrothermal system induced by the 1850 Ma Sudbury impact event. *Geology* **26**, 447–450.

Barnhart C. J., Nimmo F. and Travis B. J. (2010) Martian post-impact hydrothermal systems incorporating freezing. *Icarus* **208**, 101–117.

Becker K. H., Cemic L. and Langer K. (1983) Solubility of corundum in supercritical water. *Geochim. Cosmochim. Acta* **47**, 1573–1578.

Bernal J. D. (1949) The physical basis of life. *Proc. Phys. Soc. A* **62**, 537–558.

Brearley A. J. (1997) Disordered biopyriboles, amphibole, and talc in the allende meteorite: products of nebular or parent body aqueous alteration? *Science* **276**, 1103–1105.

Brearley A. J. (2006) The action of water. In *Meteorites and The Early Solar System II* (eds. D. S. Lauretta and H. Y. McSween). The University of Arizona Press, Tucson, pp. 587–624.

Brearley A. J., Rubie D. C. and Ito E. (1992) Mechanisms of the transformations between the α-polymorphs, β-polymorphs and γ-polymorphs of Mg_2SiO_4 at 15 GPa. *Phys. Chem. Miner.* **18**, 343–358.

Bridges J. C. and Grady M. M. (2000) Evaporite mineral assemblages in the nakhlite (Martian) meteorites. *Earth Planet. Sci. Lett.* **176**, 267–279.

Brown J. M. and Furnish M. D. (1987) Thermodynamics for (Mg, Fe)$_2SiO_4$ from the Hugoniot. In *High-Pressure Research in Mineral Physics* (eds. M. Manghnani and Y. Syono). Terra Sci. Pub. Comp., Tokyo, pp. 373–384.

Cavosie A. J., Valley J. W. and Wilde S. A. (2005) Magmatic $\delta^{18}O$ in 4400–3900 Ma detrital zircons: a record of the alteration and recycling of crust in the Early Archean. *Earth Planet. Sci. Lett.* **235**, 663–681.

Changela H. G. and Bridges J. C. (2010) Secondary minerals in the nakhlites formed at varying depths in an impact hydrothermal cell. *Lunar Planet. Sci. XXXXI*. Lunar Planet. Inst., Houston. #1407 (abstr.).

Ciesla F. J., Lauretta D. S., Cohen B. A. and Hood L. L. (2003) A nebular origin for chondritic fine-grained phyllosilicates. *Science* **299**, 549–552.

Cleaves H. J., Aubrey A. D. and Bada J. L. (2009) An evaluation of the critical parameters for abiotic peptide synthesis in submarine hydrothermal systems. *Origins Life Evol. Biosph.* **39**, 109–126.

Cronin J. R. and Moore C. B. (1971) Amino acid analyses of Murchison, Murray, and Allende carbonaceous chondrites. *Science* **172**, 1327–1329.

Cronin J. R. and Pizzarello S. (1997) Enantiomeric excesses in meteoritic amino acids. *Science* **275**, 951–955.

Culler T. S., Becker T. A., Muller R. A. and Renne P. R. (2000) Lunar impact history from $^{40}Ar/^{39}Ar$ dating of glass spherules. *Science* **287**, 1785–1788.

Dai C. D., Jin X. G., Fu S. Q., Shi S. C. and Wang D. D. (1997) The equation-of-states of Jilin ordinary chondrite and Nandan iron meteorite. *Sci. China Ser. D Earth Sci.* **40**, 403–410.

Dypvik H. and Jansa L. F. (2003) Sedimentary signatures and processes during marine bolide impacts: a review. *Sed. Geol.* **161**, 309–337.

Ferrière L., Koeberl C., Ivanov B. A. and Reimold W. U. (2008) Shock metamorphism of Bosumtwi impact crater rocks, shock attenuation, and uplift formation. *Science* **322**, 1678–1681.

Ferris J. P., Hill A. R., Liu R. H. and Orgel L. E. (1996) Synthesis of long prebiotic oligomers on mineral surfaces. *Nature* **381**, 59–61.

Fritz J., Artemieva N. and Greshake A. (2005) Ejection of Martian meteorites. *Meteorit. Planet. Sci.* **40**, 1393–1411.

Furukawa Y., Nakazawa H., Sekine T. and Kakegawa T. (2007) Formation of ultrafine particles from impact-generated supercritical water. *Earth Planet. Sci. Lett.* **258**, 543–549.

Furukawa Y., Sekine T., Oba M., Kakegawa T. and Nakazawa H. (2009) Biomolecule formation by oceanic impacts on early Earth. *Nat. Geosci.* **2**, 62–66.

Gerasimov M. V., Dikov Y. P., Yakovlev O. I. and Wlotzka F. (2002) Experimental investigation of the role of water in impact vaporization chemistry. *Deep-Sea Res. II* **49**, 995–1009.

Grimm R. E. and McSween H. Y. (1989) Water and the thermal evolution of carbonaceous chondrite parent bodies. *Icarus* **82**, 244–280.

Hanss R. E., Montague B. R., Davis M. K. and Galindo C. (1978) X-ray diffractometer studies of shocked materials. In *Proc. Lunar Sci. Conf. 9th*. Lunar Planet. Inst., Houston. pp. 2773–2787.

Hedges J. I. and Hare P. E. (1987) Amino acid adsorption by clay minerals in distilled water. *Geochim. Cosmochim. Acta* **51**, 255–259.

Huber C. and Wächtershäuser G. (2006) A-hydroxy and α-amino acids under possible Hadean, volcanic origin-of-life conditions. *Science* **314**, 630–632.

Irifune T., Kubo N., Isshiki M. and Yamasaki Y. (1998) Phase transformations in serpentine and transportation of water into the lower mantle. *Geophys. Res. Lett.* **25**, 203–206.

Ivanov B. A. and Pierazzo E. (2011) Impact cratering in H_2O-bearing targets on Mars: thermal field under craters as starting conditions for hydrothermal activity. *Meteorit. Planet. Sci.* **46**, 601–619.

Jeanloz R., Ahrens T. J., Lally J. S., Nord G. L., Christie J. M. and Heuer A. H. (1977) Shock-produced olivine glass: first observation. *Science* **197**, 457–459.

Joreau P., Leroux H. and Doukhan J. C. (1997) A transmission electron microscope investigation of shock metamorphism in olivine of the Ilafegh 013 chondrite. *Meteorit. Planet. Sci.* **32**, 309–316.

Keller L. P. and Buseck P. R. (1990) Aqueous alteration in the Kaba CV3 carbonaceous chondrite. *Geochim. Cosmochim. Acta* **54**, 2113–2120.

Keller L. P., Thomas K. L., Clayton R. N., Mayeda T. K., Dehart J. M. and McKay D. S. (1994) Aqueous alteration of the Bali CV3 chondrite: evidence from mineralogy, mineral chemistry, and oxygen isotopic compositions. *Geochim. Cosmochim. Acta* **58**, 5589–5598.

Kohlstedt D. L., Goetze C., Durham W. B. and Van der Sande J. B. (1976) New technique for decorating dislocations in olivine. *Science* **191**, 1045–1046.

Kraus R. G., Stewart S. T., Seifter A. and Obst A. W. (2010) Shock and post-shock temperatures in an ice-quartz mixture: implications for melting during planetary impact events. *Earth Planet. Sci. Lett.* **289**, 162–170.

Krot A. N., Scott E. R. D. and Zolensky M. E. (1997) Origin of fayalitic olivine rims and lath-shaped matrix olivine in the CV3 chondrite Allende and its dark inclusions. *Meteorit. Planet. Sci.* **32**, 31–49.

Lange M. A., Lambert P. and Ahrens T. J. (1985) Shock effects on hydrous minerals and implications for carbonaceous meteorites. *Geochim. Cosmochim. Acta* **49**, 1715–1726.

Langenhorst F., Joreau P. and Doukhan J. C. (1995) Thermal and shock metamorphism of the Tenham chondrite: a TEM examination. *Geochim. Cosmochim. Acta* **59**, 1835–1845.

Leroux H., Doukhan J. C. and Langenhorst F. (1994) Microstructural defects in experimentally shocked diopside: a TEM characterization. *Phys. Chem. Miner.* **20**, 521–530.

Müller W. F. and Hornemann U. (1969) Shock-induced planar deformation structures in experimentally shock-loaded olivines and in olivines from chondritic meteorites. *Earth Planet. Sci. Lett.* **7**, 251–264.

Macpherson G. J., Davis A. M. and Zinner E. K. (1995) The distribution of ^{26}Al in the early solar-system: a reappraisal. *Meteoritics* **30**, 365–386.

Madon M. and Poirier J. P. (1983) Transmission electron microscope observation of α, β and γ $(Mg, Fe)_2SiO_4$ in shocked meteorites: planar defects and polymorphic transitions. *Phys. Earth Planet. Inter.* **33**, 31–44.

Martin H. (1994) Archean grey gneisses and the genesis of continental crust. In *Archean Crustal Evolution* (ed. K. C. Condie). Elsevier Sci., Amsterdam, pp. 205–247.

Marzo G. A., Davila A. F., Tornabene L. L., Dohm J. M., Fairen A. G., Gross C., Kneissl T., Bishop J. L., Roush T. L. and McKay C. P. (2010) Evidence for Hesperian impact-induced hydrothermalism on Mars. *Icarus* **208**, 667–683.

Miller S. L. (1953) A production of amino acids under possible primitive earth conditions. *Science* **117**, 528–529.

Milner D. J., Baldwin E. C. and Burchell M. J. (2008) Laboratory investigations of marine impact events: factors influencing crater formation and projectile survivability. *Meteorit. Planet. Sci.* **43**, 2015–2026.

Moody J. B. (1976) An experimental study on the serpentinization of iron-bearing olivines. *Can. Mineral.* **14**, 462–478.

Mukhin L. M., Gerasimov M. V. and Safonova E. N. (1989) Origin of precursors of organic molecules during evaporation of meteorites and mafic terrestrial rocks. *Nature* **340**, 46–48.

Nakamura T. (2005) Post-hydration thermal metamorphism of carbonaceous chondrites. *J. Mineral. Petrol. Sci.* **100**, 260–272.

Nakamura T., Noguchi T., Zolensky M. E. and Tanaka M. (2003) Mineralogy and noble-gas signatures of the carbonate-rich lithology of the Tagish Lake carbonaceous chondrite: evidence for an accretionary breccia. *Earth Planet. Sci. Lett.* **207**, 83–101.

Nakato A., Nakamura T., Kitajima F. and Noguchi T. (2008) Evaluation of dehydration mechanism during heating of hydrous asteroids based on mineralogical and chemical analysis of naturally and experimentally heated CM chondrites. *Earth Planets Space* **60**, 855–864.

Nakazawa H. (2006) *Origin of life scenario written by the Earth*. Shin-Nihon Shuppan Ltd., Tokyo, pp. 143–160 (in Japanese).

Nakazawa H., Sekine T., Kakegawa T. and Nakazawa S. (2005) High yield shock synthesis of ammonia from iron, water and nitrogen available on the early Earth. *Earth Planet. Sci. Lett.* **235**, 356–360.

Naumov M. V. (2005) Principal features of impact-generated hydrothermal circulation systems: mineralogical and geochemical evidence. *Geofluids* **5**, 165–184.

Noguchi T., Nakamura T., Misawa K., Imae N., Aoki T. and Toh S. (2009) Laihunite and jarosite in the Yamato 00 nakhlites: alteration products on Mars? *J. Geophys. Res.* **114**, E10004. doi: 10.1029/2009JE003364.

Ohnishi I. and Tomeoka K. (2007) Hydrothermal alteration experiments of enstatite: implications for aqueous alteration of carbonaceous chondrites. *Meteorit. Planet. Sci.* **42**, 49–61.

Osinski G. R., Lee P., Parnell J., Spray J. G. and Baron M. T. (2005) A case study of impact-induced hydrothermal activity: the Haughton impact structure, Devon Island, Canadian high arctic. *Meteorit. Planet. Sci.* **40**, 1859–1877.

Proskurowski G., Lilley M. D., Seewald J. S., Fruh-Green G. L., Olson E. J., Lupton J. E., Sylva S. P. and Kelley D. S. (2008) Abiogenic hydrocarbon production at lost city hydrothermal field. *Science* **319**, 604–607.

Reimold W. U. and Stöffler D. (1978) Experimental shock metamorphism of dunite. In *Proc. Lunar Sci. Conf. 9th*, pp. 2805–2824.

Rice M. H. and Walsh J. M. (1957) Equation of state of water to 250 kilobars. *J. Chem. Phys.* **26**, 824–830.

Sasaki M., Fang Z., Fukushima Y., Adschiri T. and Arai K. (2000) Dissolution and hydrolysis of cellulose in subcritical and supercritical water. *Ind. Eng. Chem. Res.* **39**, 2883–2890.

Schoenberg R., Kamber B. S., Collerson K. D. and Moorbath S. (2002) Tungsten isotope evidence from similar to 3.8-Gyr metamorphosed sediments for early meteorite bombardment of the Earth. *Nature* **418**, 403–405.

Schwenzer S. P. and Kring D. A. (2009) Impact-generated hydrothermal systems capable of forming phyllosilicates on Noachian Mars. *Geology* **37**, 1091–1094.

Scott E. R. D., Keil K. and Stöffler D. (1992) Shock metamorphism of carbonaceous chondrites. *Geochim. Cosmochim. Acta* **56**, 4281–4293.

Snow J. E. and Dick H. J. B. (1995) Pervasive magnesium loss by marine weathering of peridotite. *Geochim. Cosmochim. Acta* **59**, 4219–4235.

Stöffler D., Keil K. and Scott E. R. D. (1991) Shock metamorphism of ordinary chondrites. *Geochim. Cosmochim. Acta* **55**, 3845–3867.

Stewart S. T. and Ahrens T. J. (2005) Shock properties of H_2O ice. *J. Geophys. Res.* **110**, E03005. doi: 10.1029/2004JE002305.

Sugita S. and Schultz P. H. (2003a) Interactions between impact-induced vapor clouds and the ambient atmosphere: 1. Spectroscopic observations using diatomic molecular emission. *J. Geophys. Res.* **108**, E65051. doi: 10.1029/2002JE001959.

Sugita S. and Schultz P. H. (2003b) Interactions between impact-induced vapor clouds and the ambient atmosphere: 2. Theoretical modeling. *J. Geophys. Res.* **108**, E65052. doi:10.1029/2002JE001960.

Taylor S. R. and McLennan S. M. (1995) The geochemical evolution of the continental crust. *Rev. Geophys.* **33**, 241–265.

Tomeoka K. and Buseck P. R. (1988) Matrix mineralogy of the Orgueil CI carbonaceous chondrite. *Geochim. Cosmochim. Acta* **52**, 1627–1640.

Tomeoka K. and Buseck P. R. (1990) Phyllosilicates in the Mokoia CV carbonaceous chondrite: evidence for aqueous alteration in an oxidizing environment. *Geochim. Cosmochim. Acta* **54**, 1745–1754.

Tomioka N., Tomeoka K., Nakamura-Messenger K. and Sekine T. (2007) Heating effects of the matrix of experimentally shocked Murchison CM chondrite: comparison with micrometeorites. *Meteorit. Planet. Sci.* **42**, 19–30.

Treiman A. H., Barrett R. A. and Gooding J. L. (1993) Preterrestrial aqueous alteration of the Lafayette (SNC) meteorite. *Meteoritics* **28**, 86–97.

Ulmer P. and Trommsdorff V. (1995) Serpentine stability to mantle depths and subduction-related magmatism. *Science* **268**, 858–861.

Valley J. W., Peck W. H., King E. M. and Wilde S. A. (2002) A cool early Earth. *Geology* **30**, 351–354.

Wegner W. W. and Ernst W. G. (1983) Experimentally determined hydration and dehydration reaction rates in the system MgO–SiO_2–H_2O. *Am. J. Sci.* **283-A**, 151–180.

Weisberg M. K., Zolensky M. E. and Prinz M. (1997) Fayalitic olivine in matrix of the Krymka LL3.1 chondrite: vapor-solid growth in the solar nebula. *Meteorit. Planet. Sci.* **32**, 791–801.

Wilde S. A., Valley J. W., Peck W. H. and Graham C. M. (2001) Evidence from detrital zircons for the existence of continental crust and oceans on the Earth 4.4 Gyr ago. *Nature* **409**, 175–178.

Williamson G. K. and Hall W. H. (1953) X-ray line broadening from filed aluminium and wolfram. *Acta Metall.* **1**, 22–31.

Yada K. and Iishi K. (1974) Serpentine minerals hydrothermally synthesized and their microstructures. *J. Cryst. Growth* **24**, 627–630.

Yada K. and Iishi K. (1977) Growth and microstructure of synthetic chrysotile. *Am. Mineral.* **62**, 958–965.

Associate editor: W. Uwe Reimold